phys. stat. sol. (b) **191**, 369 (1995)

Subject classification: 71.25; 62.20; S5; S7

Sektion Physik der Universität München[1])

Calculation of the Ground State Properties of Diamond and Cubic Boron Nitride

By

H. BROSS and R. BADER

(Received February 24, 1995; in revised form May 22, 1995)

Using the modified augmented plane wave method (MAPW), the ground state properties of cubic boron nitride and diamond are investigated within the framework of the local density approximation (LDA). As is common for LDA, the value of the band gap is underestimated by the one-particle excited states. Calculation of the total energy as a function of the lattice parameter yields equilibrium lattice constants within 1% of the experimental value. Furthermore, the hydrostatic bulk moduli obtained deviate from the experimental values by about 10% in the case of BN and 4% in the case of diamond. An estimate of the cohesion energy of both materials is obtained from the atomic limit within the MAPW scheme yielding improved values when compared to the difference between crystal and single atom LDA total energies.

Mit Hilfe des MAPW-Verfahrens werden im Rahmen der lokalen Dichte-Näherung Grundzustandseigenschaften der Halbleiter Bornitrid (Zinkblendestruktur) und Diamant bestimmt. Wie für LDA üblich, wird der Wert der Bandlücke durch die Einteilchen-Anregungsenergien unterschätzt. Die Berechnung der Gesamtenergie als Funktion der Gitterkonstante liefert Übereinstimmung mit dem experimentellen Wert der Gitterkonstante bis auf 1%. Der hydrostatische Kompressionsmodul weicht bei Bornitrid um 10% und bei Diamant um 4% vom Experiment ab. Eine Abschätzung der Kohäsionsenergie der beiden Materialien wird aus den MAPW-Ergebnissen im Grenzfall $a \to \infty$ gewonnen; sie liefert gegenüber dem direkten Vergleich mit atomaren LDA-Resultaten verbesserte Werte.

1. Introduction

The isoelectronic compounds boron nitride, BN, and diamond, C, crystallize in the zincblende and diamond lattice, respectively. Both materials are of technological interest because of their mechanical properties, their high melting point, and low dielectric constant, making them useful for protective coatings. Their electronic properties, especially the high value for their band gap, seem to hold promise for use in electronic devices working under high temperature conditions.

The first theoretical study of electronic properties of diamond was performed by Herman [1], for boron nitride this was achieved bei Kleinman and Phillips [2]. Later investigations with increasing precision have been performed for boron nitride by Zunger and Freeman [3] using the LCAO method, by Wentzcovich et al. [4] using a pseudopotential method, and more recently by Xu and Ching [5], who obtained their results with the orthogonalized LCAO method, and additionally evaluated optical properties from their self-consistent potentials. More recent studies on diamond were published by Zunger and Freeman [6]

[1]) Theresienstr. 37/IV, D-80333 München, Federal Republic of Germany.

and Chelikowsky and Louie [7], both papers being based on the LCAO method, by van Camp et al. [8], who employed the ab initio nonlocal norm-conserving pseudopotential method to calculate pressure-dependent ground state properties. Data on band energies of diamond from a fully self-consistent pseudopotential calculation are to be found in a paper by Surh et al. [9]. A LDA pseudopotential method was also used for self-consistent calculations some years earlier by Yin and Cohen [10]. The newest results on the charge distribution in diamond are presented by Lu and Zunger [11], who give an overview of experimental and theoretical values, including their own LAPW results.

The investigations presented here are motivated by the fact that previous calculations have incorporated computational approximations whose effects on the electronic structure, on the charge density, and on the total energy remain, in many cases, untested. These include the pseudopotential approximation which does not properly describe the rapid oscillations of the wave function near the nuclei, and the linear muffin-tin orbital (LMTO) calculations which use a rather limited basis set. The modified augmented plane wave (MAPW) scheme by one of the authors [12 to 14] is, apart from the one-particle approximation, free of any systematic errors as it allows by suitable choice of the characteristic parameters of the scheme any accuracy wanted. Without being complete it has the following merits:

1. both wave function and its gradient are strictly continuous throughout the crystal;
2. it is a linear method which treats on equal footing both the core and valence electrons. Thus *all* states obtained for a fixed value of the wave vector $\boldsymbol{k}$ are strictly orthogonal to each other. In this respect it is an all-electron scheme;
3. the wave functions obtained by the scheme show the correct rapid oscillations near the nuclei caused by the Coulomb singularity of the crystal potential;
4. up to the contributions due to the nonspherical potential within the atomic spheres all sums defining the total charge density, the total energy, and the matrix elements of the eigenvalue problem turn out to be finite. Thus, no truncation errors occur.

Due to these advantages the wave functions obtained by use of the MAPW scheme are of high accuracy and are especially suited for further investigations, e.g. the evaluation of the dielectric function or of Wannier functions. Details of the MAPW scheme for a Bravais lattice are described elsewhere [15]. In the Appendix we sketch how this scheme is adapted to treat a lattice with a basis.

2. Application of the MAPW Method to Boron Nitride and Diamond

Apart from the total energy investigations based on application of hydrostatic pressure, the ground state properties were calculated with the experimental lattice parameter values a^{expt} of 6.740 and 6.832 atomic units (a.u.) for diamond and boron nitride, respectively. For both materials treated the two APW spheres were chose equal, with radius $r_0 = \sqrt{3}/8a$. The unit cell volume is $V_c = \frac{1}{4}a^3$. The APW spheres occupy $\approx 34\%$ of the unit cell, the remaining 66% are henceforth called interstitial region. In order to obtain one-particle band energies converged to better than 0.2 mRyd for all occupied bands, for each of the ten special points $\boldsymbol{k}$ in the irreducible wedge of the Brillouin zone, all plane waves with wave vectors obeying

$$\left(\frac{a}{2\pi}\right)^2 |\boldsymbol{k} + \boldsymbol{K}|^2 \leqq 34.9 \tag{2.1}$$

were included in the MAPW ansatz, yielding between 213 and 219 ansatz functions depending on the integration point coordinates. This is to be contrasted with about 60 plane waves for the case of f.c.c. Cu, whose close packed structure possesses an interstitial region of only 26%. The augmentation was performed using five radial functions with angular momentum 0 and four functions with angular momentum 1 in each APW sphere. With the exception of the 1s state, which was included in the MAPW space as a pure bound state, the first regular solutions of the radial equation whose energies E are determined by

$$\frac{\mathrm{d}}{\mathrm{d}r} \ln R(r; E)\,|_{r=r_0} = \pm 1 \tag{2.2}$$

were used. In this way one obtains between 247 and 253 expansion coefficients. By introducing the side conditions (A) the dimension of the ansatz space is effectively reduced to 231 to 237. This size of the eigenvalue problem has to be contrasted with the corresponding size of the pseudopotential method where the cutoff in the kinetic energy given by the right-hand side of (2.1) was chosen up to 75 yielding more than 900 plane waves.

For each material, self-consistent potentials were obtained for a numbers of lattice parameters according to the prescription given in the Appendix. The results obtained from these are described in the following section.

3. Results

3.1 Band structure and density of states

The band structures of C and BN are displayed in Fig. 1 and 2, respectively. The energy scale was fixed by prescribing

$$\hat{V}(\boldsymbol{K} = 0) = \int_{\Omega} V(\boldsymbol{r})\,\mathrm{d}^3 r = 0\,. \tag{3.1}$$

Both materials are characterized by valence hybridization yielding four valence bands separated from a closed complex of the first four conduction bands by a band gap which is a direct one for BN ($X_c \to \Gamma_v$) and an indirect one for C ($\Delta_c \to \Gamma_v$), the conduction band minimum being located at $\boldsymbol{k}_{\min} = 2\pi/a(0.719, 0, 0)$. The experimental value is $k_x = 0.76(1)$ [16]. For both materials another band gap occurs between the fourth and the higher conduction bands. This appears due to the fact that all contributing atoms are from the first period; it probably does not have any grounding in experimental evidence as the density functional theory cannot make any statement about excited states.

The essential difference between the band structures of diamond and BN is the split-off of the lowest valence band in the case of BN. The reason for this is that the symmetry of the diamond structure enforces the existence of exactly one two-dimensional representation on the highly symmetrical direction Z, while the zincblende structure possesses two one-dimensional representations. It is only on this set of measure zero that the lowest and second lowest valence bands of diamond merge. Another interesting difference between the two materials concerns their 1s states: The nearly degenerate 1s bands of diamond located at about -17.332 Ryd show a dispersion of nearly 1 mRyd displayed in the lower part of Fig. 1, whereas in boron nitride the 1s states of boron at -10.72971 Ryd and of nitrogen at -25.50254 Ryd, respectively, are far better localized with a variation of less than 0.01 mRyd throughout the Brillouin zone. The reason for this is the following: The 1s

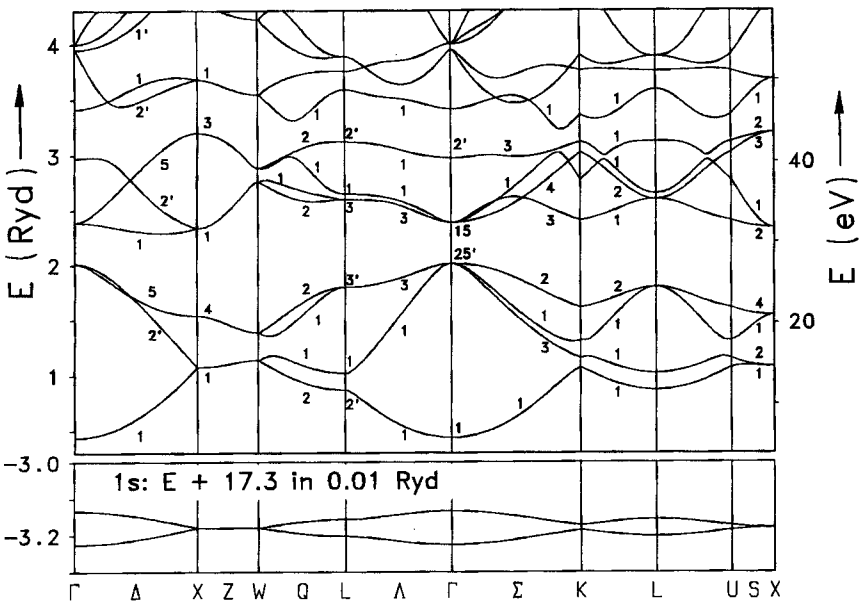

Fig. 1. Self-consistent band structure of diamond on highly symmetric directions in the first Brillouin zone. The upper box shows the four uppermost valence bands and the first few conduction bands, while the lower one displays the 1s dispersion. See text for choice of energy zero. The experimental lattice parameter value of 6.74 a.u. was used

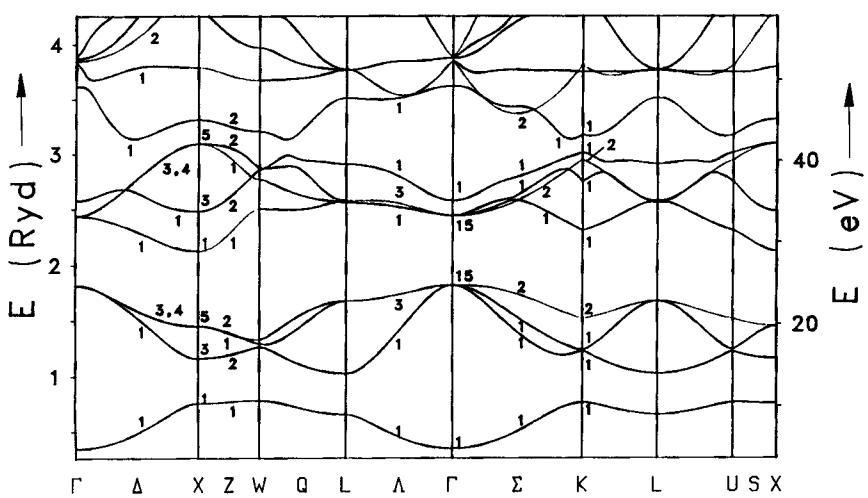

Fig. 2. Self-consistent band structure of cubic BN on highly symmetric directions in the first Brillouin zone. The four uppermost valence bands and the first few conduction bands are drawn. See text for choice of energy zero. The experimental lattice parameter value of 6.832 a.u. was used

states of boron and nitrogen are localized at the nuclei on the respective f.c.c. sublattice sites, yielding an effective nearest-neighbour distance of $a/\sqrt{2} = 4.83$ a.u., thus making electron propagation throughout the crystal impossible, while in the case of diamond the two sublattices interact because of the 1s energy being the same for both of them, resulting in an effective nearest-neighbour distance of $a\sqrt{3}/4 = 2.92$ a.u.

Comparison of the general topology of the diamond band structure with Fig. 4 of [7] reveals an overall agreement (apart from two classification faults in the reference). For a few characteristic points of the Brillouin zone, the band energies of diamond are displayed in the lower part of Table 1 for both the experimental and equilibrium lattice parameter values. As far as transitions from the conduction to the valence bands are concerned, it is interesting to observe the downward trend from the earliest (LCAO [6]) to our most recent value prevailing with the exception of $X_{4c} \rightarrow \Gamma'_{25v}$. However, we expect the values obtained by us to be distinctly too small due to the neglection of nonspherical potential contributions as experience in the case of silicon has shown [17]. With the valence bands, the trend is in the opposite direction. Noteworthy is the very weak dependence of the indirect gap value on the lattice parameter. In Table 1, we have included the experimental results of Himpsel

Table 1
Band gaps, bandwidths, and band energies at special points. All energy values are in eV

boron nitride:	our results*)		OLCAO [5]	pseudop. [4]	expt.
	a^0	a^{expt}	a^{expt}	$a = 6.814$	
indirect gap $X_{1c} \rightarrow \Gamma_{15v}$	4.199	4.165	5.18	4.2	$<6.0 \pm 0.5$ [35], 6.4 [36]
direct gap $\Gamma_{15c} \rightarrow \Gamma_{15v}$	8.612	8.438	8.7	8.6	14.5 [37]
$X_{1c} \rightarrow X_{5v}$	9.392	9.150	10.3	–	–
$L_{1c} \rightarrow L_{3v}$	12.626	12.007	12.4	–	–
$L_{3c} \rightarrow L_{3v}$	12.540	12.255	–	–	–
$K_{1c} \rightarrow K_{2v}$	11.052	10.763	11.8	–	–
upper val. band: $\Gamma_{15v} \rightarrow L_{1v}$	11.180	10.793	10.94	10.8	–
lower val. band: $\Gamma_{1v} \rightarrow W$	6.302	6.015	6.92	5.9	–
total valence band:	20.607	20.134	21.1	20.3	>20.8 [35]

diamond:	our results		pseudop. [9]	LCAO [6]	expt. [18]
	a^0	a^{expt}		a^{expt}	
indirect gap $\Delta_{1c}^{min} \rightarrow \Gamma'_{25v}$	3.899	3.820	3.9	5.45	5.5 ± 0.05
direct gap $\Gamma_{15c} \rightarrow \Gamma'_{25v}$	5.224	5.140	5.5	6.33	6.0 ± 0.2
$X_{1c} \rightarrow \Gamma'_{25v}$	4.528	4.461	–	8.96	–
$X_{4c} \rightarrow \Gamma'_{25v}$	16.706	16.174	–	16.69	–
$\Gamma'_{2c} \rightarrow \Gamma'_{25v}$	13.940	13.129	13.1	14.07	15.3 ± 0.5
$X'_{1v} \rightarrow \Gamma'_{25v}$	−12.996	−12.73	–	−12.17	–
$X_{4v} \rightarrow \Gamma'_{25v}$	−6.649	−6.506	–	−6.09	–
$L'_{2v} \rightarrow \Gamma'_{25v}$	−15.876	−15.604	−15.8	−15.17	-15.2 ± 0.3
$L_{1v} \rightarrow \Gamma'_{25v}$	−13.929	−13.510	−13.6	−12.18	-12.8 ± 0.3
$L'_{3v} \rightarrow \Gamma'_{25v}$	−2.965	−2.866	–	−2.82	–
total valence band:	21.947	21.458	21.7	20.44	21 ± 1

*) a^0 and a^{expt} are the theoretical and experimental lattice parameters (in a.u.) given in Table 5 for both materials

et al. [18], who used *hv*-dependent photoemission to determine the one-particle bulk energies. For occupied states reasonable consistency with our results is observed; the prediction for the total valence band width is within the experimental error. As is common for density functional schemes, excited states cannot be described correctly: the band gap is estimated at 70% of the experimental value.

The BN band structure was compared with the one displayed in [5]. Generally, the band shapes agree very well, the main difference being the value of the band gap as displayed in the upper part of Table 1. Comparison with the pseudopotential band structure from [4] appears problematic because the evaluation was performed with the author's equilibrium lattice parameter value of 6.814 a.u. In Table 1 results for both the experimental and our theoretical lattice parameters are given. It again turns out that the value of the band gap shows only weak dependence on a; agreement with the pseudopotential results is therefore reasonably good for both parameter values. Other band energy differences proved to be far more sensitive to the variation of the lattice parameter, however, the most characteristic change being a change of order of the L_{1c} and L_{3c} levels in the lowest conduction band complex. This phenomenon also has been noted by Zunger and Freeman [3] who, however, obtained the zero of L_{1c}–L_{3c} at about $a = 6.54$ a.u., a far lower value than our equilibrium one, possibly due to their use of X_α potentials.

For some of the highly symmetric points in the Brillouin zone, the band masses with respect to some specific directions were calculated. The results are given in Table 2. In the

Table 2

Band masses of the uppermost conduction and the lowest valence bands at some highly symmetric points of the first Brillouin zone. All values are given in units of the electron mass. See the band structures for names of representations

location and direction	diamond		boron nitride	
	this work	expt. [19]	this work	Xu and Ching [5]
Γ'_{25v} viz. $\Gamma_{15v} \to X$	−0.27; −0.52	–	−0.51; −0.52	−0.54; −0.55
Γ'_{25v} viz. $\Gamma_{15v} \to K$	−0.20; −0.27; −2.04	–	−0.27; −0.51; −4.02	−0.44; −0.64; −3.16
Γ'_{25v} viz. $\Gamma_{15v} \to \Lambda$	−0.16; −0.65	–	−0.24; −1.22	−0.36; −1.20
$\Gamma_{15c} \to X$	−1.75; 0.23	–	−0.89; 0.40	–
$\Gamma_{15c} \to K$	1.27; 0.34	–	1.77; 1.18; 0.40	–
$\Gamma_{15c} \to \Lambda$	0.51; 0.24	–	0.82; 0.67	–
$\Delta_{1c}^{min} \to \Gamma$	1.73	1.4	–	–
$\Delta_{1c}^{min} \perp \Gamma$	0.29	0.36	–	–
X_{4c} viz. $X_{5c} \to W$	−0.55	–	0.30	–
X_{4c} viz. $X_{5c} \to U$	−0.23; 1.51	–	0.30	–
$X_{5c} \to K$	–	–	0.30	0.26
$X_{5c} \to \Gamma$	–	–	1.42	1.20
$X_{1v} \to W$	0.31	–	–	–
$X_{1v} \to U$	1.61; 1.70	–	–	–
$X_{5v} \to K$	–	–	−0.36; −4.39	–
$X_{5v} \to \Gamma$	–	–	0.91	–
L'_{3c} viz. $L_{3c} \to \Gamma$	2.01	–	2.44	–
L'_{3c} viz. $L_{3c} \to W$	−0.27; −0.72	–	−0.33; −0.90	–
L_{3v} viz. $L_{1v} \to \Gamma$	−18.28	–	−3.51	–
L_{3v} viz. $L_{1v} \to W$	−1.32; 0.39	–	0.49	–

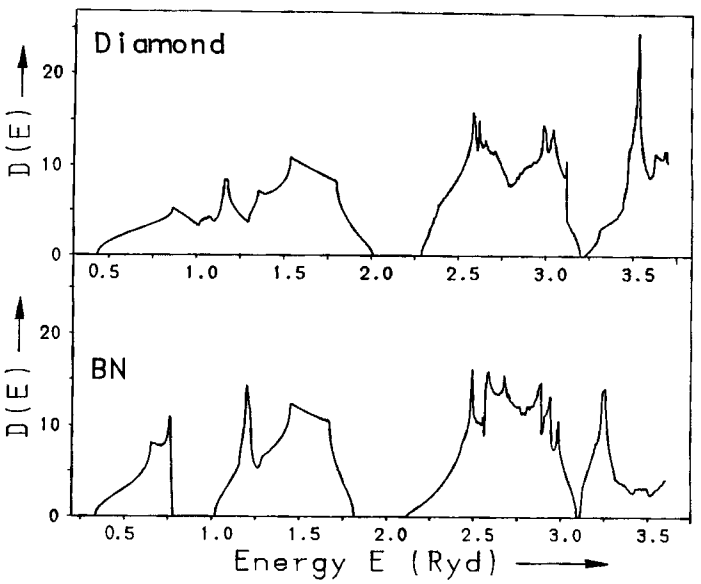

Fig. 3. Density of states (in electrons/Ryd) for diamond and boron nitride. The calculation was performed using 2480 special points in the f.c.c. Brillouin zone in each case. The energy axis of the lower graph is shifted to the right by 0.1 Ryd with respect to the upper

case of diamond, experimental values by Nava et al. [19] on the conduction band masses on $\Delta_{1\,\min}$ were available for comparison. It appears that our calculation overestimates the longitudinal mass and underestimates the transverse one. For BN our results are compared with Xu and Ching's theoretical values; deviations up to 20% occur.

The density of states (DOS) of C and BN,

$$D(E) = 2\frac{V_c}{(2\pi)^3}\int_{1.\mathrm{BZ}}\sum_{n\in\mathrm{occ.}}\delta(E - E_{nk})\,\mathrm{d}^3k \tag{3.2}$$

are displayed in Fig. 3. The k-integral was discretized using 2480 special points in the irreducible wedge of the first Brillouin zone. Furthermore the improved Gilat-Raubenheimer method [20 to 22] was again used, requiring $\nabla_k E_{nk}$ as input. For the BN DOS the overall topology of the valence band contributions agrees with that found in [5] although our curve appears to be smoother, indicating a higher precision of the k-space integration. No reference was found displaying a DOS based on an LDA calculation in the case of diamond. Comparing the DOS of diamond and BN reveals a narrower valence band complex of BN and a steeper slope of the first conduction band contribution of diamond. The second band gaps again are clearly identifiable in the DOS of both materials.

3.2 Electronic density

While for diamond the bonding between two nearest neighbour atoms is symmetric with respect to the symmetry plane lying between these atoms, in boron nitride there occurs a shift of electronic charge from the boron atom to the nitrogen atom revealing the higher electronegativity of nitrogen. The valence charge densities of both materials, i.e. disregarding

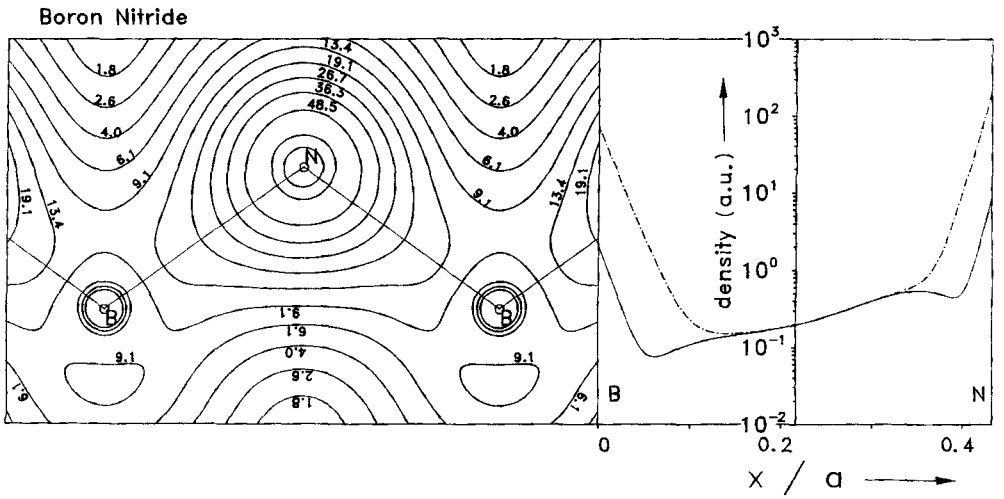

Fig. 4. Charge density maps of boron nitride. Left: Contours of the valence charge in units of 0.01 a.u. Right: the valence (solid) and total (dash-dotted) charge density displayed logarithmically along the [111] direction between nearest neighbour B and N nuclei

the 1s core of each atom, are displayed in Fig. 4 and 5 as contour plots in the (110) plane. Furthermore valence and total charge densities along the bond lines between two atoms are shown. The contour plot for BN reveals how the charge shift toward the nitrogen atom effectively increases the size of the latter in the sense that the sphericity of the charge distribution prevails in a much larger region around the N than around the B nucleus, while in the case of diamond the sp^3 orbitals localized quite near the nuclei can be clearly identified. The charge near the B nucleus in BN in fact appears to prefer the far side of the

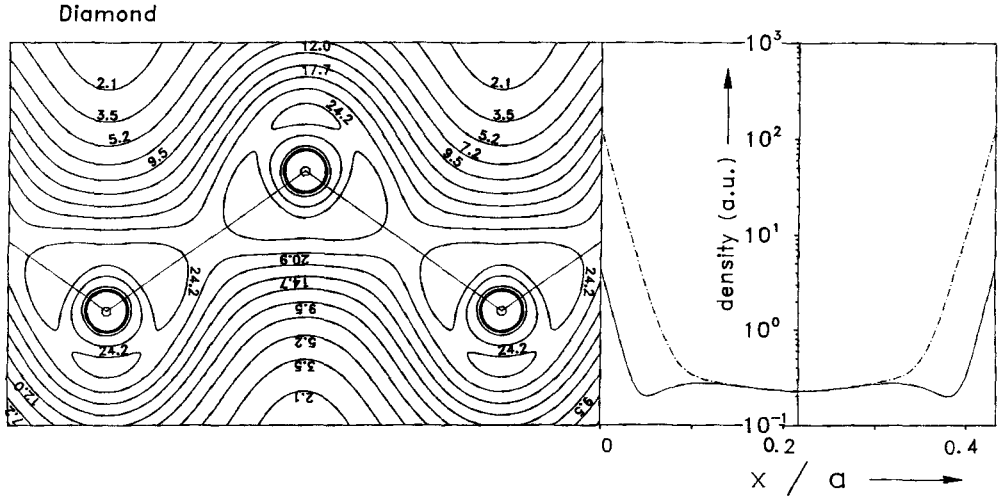

Fig. 5. Charge density maps of diamond. Left: Contours of the valence charge in units of 0.01 a.u. Right: the valence (solid) and total (dash-dotted) charge density displayed logarithmically along the [111] direction between nearest neighbours

bond. As a consequence of the purely covalent C–C bonds more charge is accumulated in the interstitial region: 3.049 electrons as opposed to 2.832 in the case of BN. The charge density of diamond along the [111] direction shows a distinct depression midway between the nuclei. This has also been reported for other calculation schemes [8, 11]. Because of the charge shift, in the case of BN no depression appears, although there is still a noticeable reduction of the increase of charge density toward the N atom. The minimum value of the valence charge density along the [111] direction for diamond is $15.24e^-$/cell at a normalized distance of $x/a = 0.052$ from the C nucleus; at the midpoint of the bond $x/a = \sqrt{3}/8$ the valence as well as the total charge density have the value $17.29e^-$/cell. Between those two minima a maximum of $21.19e^-$/cell occurs at $x/a = 0.111$, to be compared to the theoretical value $22.32e^-$/cell at distance 0.117 from the nucleus obtained by van Camp et al. [8]. Lu and Zunger [11] obtained the first minimum of the valence charge density, $15.6e^-$/cell, at normalized distance 0.050, the following maximum value of $22.0e^-$/cell at distance 0.11, and the midway minimum value of $18.0e^-$/cell. Deviations of up to 5% occur. The reasons for this are those mentioned below in the discussion of the X-ray form factors. For BN the minima have the values $5.96e^-$/cell for the B atom and $35.256e^-$/cell for the N atom at normalized distances 0.062 and 0.043, respectively, a local maximum occurring 0.080 from the N nucleus with density value $43.24e^-$/cell. No tabulated results were found in the case of BN. However, the values appear reasonably consistent with what can be inferred from Fig. 8 of Xu and Ching [5].

Tables 3 and 4 show the charge density results for both materials, comparing them with the most recent available calculations and experimental values. In the case of diamond, the static structure factors per atom appear consistent to the results of Lu and Zunger [11] within 1% and better, excepting the (222) reflection. The latter would vanish if a spherical charge density could be assigned to each C atom and therefore is a measure of the accuracy with which the nonspherical contributions of ϱ_{el} can be reproduced within the LDA. The value presented here is significantly too small, although the experimental data also vary greatly. Whether this constitutes a failure of the LDA can only be assessed after nonspherical

Table 3

Electronic charge distribution of diamond: static form factors of X-ray scattering. The charge distribution is given by the infinite Fourier series

$$\varrho_{el}(r) = \sum_{K} S(K) \cos [a/8(K_1 + K_2 + K_3)] \cos (Kr)$$

reflection	$S(K)$	LAPW [11]	expt. [38]	expt. [39]
111	3.271	3.282	3.274	3.357
220	1.977	1.976	1.962	1.982
311	1.713	1.700	1.697	1.667
222	0.089	0.111	0.149	0.114
400	1.571	1.564	1.557	1.483
331	1.546	1.558	1.562	1.587
422	1.433	1.434	1.454	1.451
333	1.372	1.364	1.385	1.427
511	1.384	1.384	1.409	1.427
440	1.314	1.316	1.306	1.294
442	0.004	–	–	–
622	0.001	–	–	–

Table 4
Electronic charge distribution of BN: static form factors of X-ray scattering. The charge distribution is given by the infinite real-valued Fourier series
$\varrho_{el}(r) = \sum_{K} S(K) \exp i(\pi x(K) + Kr)$.
$x = 1$ or 0 denotes a precise value, while $x = 1.000$ implies a truncation to three digits

reflection	$S(K)$	$x(K)$	LCAO [3]	expt. [23]	expt. [24]
111	4.941	0.332	4.97	4.92 ± 0.15	5.01 ± 0.04
200	1.481	1	1.58	1.56 ± 0.05	1.59 ± 0.04
220	4.171	0	4.17	4.17 ± 0.10	4.17 ± 0.01
311	2.571	−0.295	2.64	2.59 ± 0.10	2.59 ± 0.01
222	0.476	0.904	0.57	0.50 ± 0.02	0.50 ± 0.01
400	3.221	0	3.20	3.22 ± 0.10	3.17 ± 0.02
331	2.216	0.282	2.16	2.17 ± 0.05	2.21 ± 0.01
420	0.309	1	0.32	0.32 ± 0.01	0.316 ± 0.003
422	2.865	1.000	–	–	2.84 ± 0.02
333	1.948	−0.285	1.97	1.96 ± 0.06	1.94 ± 0.02
511	1.960	0.285	1.95	1.96 ± 0.06	1.93 ± 0.03
440	2.602	0	–	–	2.58 ± 0.01
531	1.792	−0.291	–	–	1.77 ± 0.02
442	0.331	1.000	–	–	0.340 ± 0.003

potential contributions have been taken into account self-consistently. For the case of boron nitride, the static structure factors of a unit cell are given by absolute value and phase, the latter not being accessible to measurements. Here an assessment of nonspherical contributions can only be performed by comparing reflections yielding *identical* results in case of spherical charge distributions, i.e. the (333) and (511) reflections, while the (200) reflection, vanishing for the diamond structure, can serve as a measure for the deviation from inversion symmetry with respect to the midpoint between the B and N nuclei. The fourth and fifth columns of Table 4 shows experimental results obtained by Weiss [23] and Will et al. [24], respectively. In the case of Will's results, no Debye Waller factor could be obtained for the data accessible to us. Therefore an optimal rms fit was performed using the 76 measured coefficients; a Debye-Waller factor of 0.670 yielded the best fit and was applied to the experimental values, using a common normalization factor of 0.247. The consistency between the results of Weiss and Will is within experimental error, *with exception of the (111) reflection*, for which the consistency of theoretical values suggests that Will's measurement is in error. Turning to the interpretation of our results we observe significant deviations for the (200) reflection, which we suspect to indicate that the warped muffin tin approximation does not describe the charge transfer with sufficient precision. The same occurs for most small coefficients like (222) and (420) to which the spherical part of the charge density within the APW spheres does not contribute. The overall consistency of the measured coefficients of Weiss not shown in the table with our theoretical results remains good (2% and mostly within the experimental error bars) for all large values, while the small (nonspherical) ones deviate by up to 10%.

3.3 Total energy and bulk moduli

In order to obtain the Kohn-Sham equilibrium lattice parameter, self-consistent potentials were calculated for a number of values of a and the resulting total energies fitted to a

exponential model,

$$E_{\mathrm{tot}}(V_c) = p_1 + p_2 V_c + p_3 V_c^2 + p_4 \exp(-p_5 V_c). \tag{3.3}$$

The total energy curves for both materials are displayed in Fig. 6. For diamond, 25 calculated points were fitted, for boron nitride 42. The equilibrium crystal cell volume $V_c^0(p, T = 0)$ is obtained by minimizing the free energy function,

$$\Phi_{p,T}(V, S) = E_{\mathrm{tot}}(V, T) - TS + pV, \tag{3.4}$$

for the cell volume at $T = 0$. The entropy per unit cell S therefore needs no further consideration. For external hydrostatic pressure p one obtains

$$\left.\frac{\partial E_{\mathrm{tot}}}{\partial V}\right|_{V = V_c^0,\, T = 0} + p = 0. \tag{3.5}$$

The bulk modulus is then given by

$$\varkappa = -V\frac{\partial p}{\partial V} = V\frac{\partial^2 E_{\mathrm{tot}}}{\partial V^2}, \tag{3.6}$$

taken at $T = 0$ and $V = V_c^0$. For both materials these data as well as the fitted model parameters are given in Table 5. The error given for the physical quantities reflects the numerical uncertainty, which was estimated by comparing the bulk modulus derived from the model (3.3) with the value obtained from a spline interpolation of a few values of a centering around the minimum of E_{tot}. Table 5 reveals that for both materials the bulk modulus is overestimated by the theory, in the case of BN by about 10% while for diamond the experimental value is only exceeded by about 4%.

Another observable quantity of the crystal is the pressure derivative of the bulk modulus. This quantity, which involves the third derivative of the total energy with respect to cell volume, is obtained by differentiation of the model function (3.3): The results are again displayed in Table 5, the error given being estimated by comparison to predictions by other models, i.e. the Murnaghan [25] equation of state. Again the theoretical value for BN seems to be slightly more off cue than the one for diamond, although the significance is not high because of the $\approx 10\%$ error for both calculated numbers.

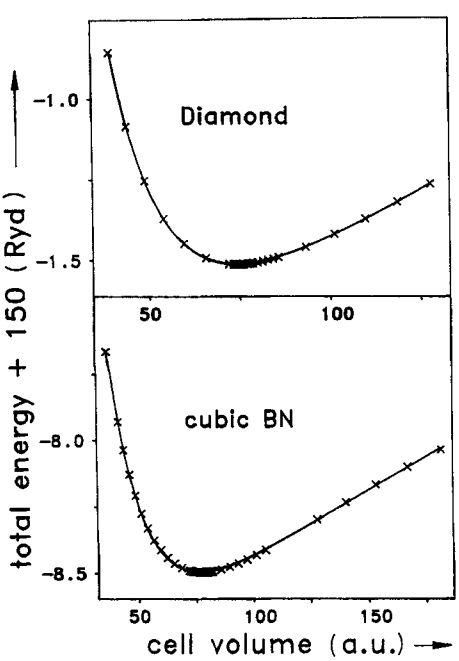

Fig. 6. Total energy curves for diamond and cubic boron nitride. Each cross corresponds to a self-consistent calculation; the line represents the fitted model discussed in the text

Table 5

Total energy results for BN and diamond. The first two sections refer to the experimental and extrapolated lattice parameters, respectively. $\varkappa$, $d\varkappa/dp$, and E_{coh} are compared with experimental values

	boron nitride		diamond	
1. $V = V_c^{expt.}$(a.u.)	79.73		76.55	
a^{expt}(a.u.)	6.832		6.740	
E_{tot} (Ryd)	−158.4935		−151.5101	
E_{kin} (Ryd)	157.0415		150.0464	
E_{pot} (Ryd)	−294.3429		−280.7148	
2. $V = V_c^0$(a.u.)	76.4		74.0	
a^0(a.u.)	6.74		6.66	
a^0/a^{expt}	0.986		0.988	
E_{tot} (Ryd)	−158.4944		−151.5111	
E_{kin} (Ryd)	157.2086		150.2281	
E_{pot} (Ryd)	−294.4657		−280.8484	
exponential model for E_{tot}:				
p_1	−159.01 ± 0.02		−152.00 ± 0.03	
$10^3 \cdot p_2$	5.8 ± 0.3		5.1 ± 0.5	
$10^6 \cdot p_3$	2.5 ± 1.2		5.7 ± 2.3	
p_4	13.71 ± 0.18		14.43 ± 0.19	
$10^2 \cdot p_5$	6.71 ± 0.05		6.94 ± 0.06	
$\varkappa(10^{11}$ Pa)	4.05 ± 0.05	3.69 ± 0.14 [26]	4.58 ± 0.05	4.42 [40]
$\frac{d\varkappa}{dp}(p = 0)$	4.2 ± 0.4	4.0 ± 0.2 [26]	4.0 ± 0.4	4.07 [40]
E_{coh} (eV/cell)	15.69	13.2 [4]	20.94	14.74 [10]

Considering the fact that the local spatial variation of the electronic density in BN is greater than in diamond, as can be inferred from Fig. 4 and 5, it is to be expected that deviations from the LDA predictions will play a greater role in the case of BN. This expectation is borne out by the above results for the bulk modulus and its pressure derivative. For the deviations of the lattice parameter this is not the case. The reason for this is that the experimental value of a at 300 K was used for both materials in order to enable a comparison with the results of [26]. For reasons of consistency, the 300 K value of the lattice parameter was also used as reference value in the case of diamond. No measurements of pressure versus volume at lower temperatures seem to have been published. As a result, any differences in the errors of the equilibrium lattice parameters of diamond and BN, respectively, are lost because of thermal effects. The thermal influence on the bulk modulus and its pressure derivative is expected to be an order of magnitude smaller [26]. A theoretical estimate of thermal effects in BN can be obtained from the Debye model. Anharmonic effects are approximately treated by a refinement of Grüneisen's method [27]. As demonstrated, e.g. in [28], the phonon contributions to the free energy are then

$$E_{vib}(V, T) = 2k_B\theta_D\left(\frac{V_0}{V}\right)^{\gamma}\left[\frac{9}{8} + \frac{3\pi^4}{5}\left(\frac{T}{\theta_D}\right)^4\left(\frac{V}{V_0}\right)^{3\gamma}\right], \tag{3.7}$$

where $\theta_D = 1800$ K is the Debye temperature and $\gamma = 1.78$ the Grüneisen parameter of BN; these phenomenological values were also used in [26] to estimate thermal effects. The

factor 2 takes the number of atoms per unit cell into account. Mainly due to the zero point motion of the lattice the equilibrium lattice parameter at 0 K is shifted to ≈ 6.791 a.u., improving the accuracy of the prediction to 99.4%. The value for the bulk modulus is also improved somewhat to 3.93×10^{11} Pa although consistently with the above reasoning there is still a deviation of nearly 7%. The pressure as a function of relative crystal volume, obtained by taking the derivative of the fitted total energy curve, also needs to be interpreted keeping the thermal effects in mind. The uncorrected curve is represented by the full line in Fig. 7; application of the thermal corrections in the case of BN leads to the broken line in the lower part of the same figure, which lies much closer to the experimental data than the original curve. The predictions from [26] correcting their theoretical curve for thermal effects in fact lead to *higher* systematic deviations. This is due to the fact that the pseudopotential method used overestimates the equilibrium lattice constant contrary to our formalism. We expect the deviations from experiments performed at low temperatures to be of the same order of magnitude but different sign for the two calculational schemes. The reasons for this could be threefold: Firstly our neglection of nonspherical contributions, secondly differing expressions for ε_c (from [26] it is not clear which one was used), thirdly the intrinsic error in the solution of the one-particle Schrödinger equation. As far as the latter point is concerned, we believe our scheme to yield the more precise results, while the first point still requires further assessment.

The cohesion energies referred to in Table 5 were calculated by comparing the total energy at V_c^0 with the total energy calculated for a lattice constant 3.6 times the equilibrium constant, using the same parameters in the band structure calculation as given in Section 2. Thus, uncertainties of the method are largely reduced: In the case of single atom

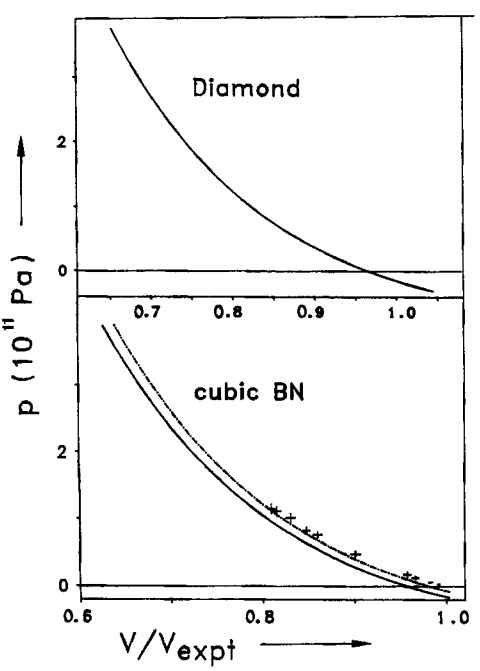

Fig. 7. Pressure vs. relative crystal volume for diamond and cubic boron nitride. The full line denotes the electron-only results at 0 K, while the broken one includes an approximation of thermal and anharmonic effects of lattice vibrations at 300 K as described in the text. V_{expt} denotes the experimentally found unit cell volume at 300 K, corresponding to the lattice parameter 6.832 a.u. The crosses in the BN drawing denote experimental values measured at 300 K including error bars. The curves were obtained by differentiation of the model function for the total energy. The zero line drawn crosses the functions at the relative equilibrium unit cell volume for the respective approximations. See discussion in the text, especially for references

calculations, the errors induced by applying the LDA to low to intermediate electron densities results in too high total energy results and therefore in a considerable overestimation of cohesion energies as discussed below. As the valence orbitals dehybridize for lattice parameters about 25% larger than the equilibrium value and develop towards the 2s and 2p states of the single atom, the occupation numbers were chosen so as to simulate two neutral atoms in the case of BN: Of the six p-like orbitals obtained by the band structure calculation those three essentially localized near the B atom were occupied with $\frac{1}{6}$ electron each, the remaining three localized at the N site with $\frac{1}{2}$ electron each. As a criterion for the atomic limit the convergence of the total energy towards a constant value was chosen: For the value 25.0 a.u. of the lattice parameter the total energy was -157.3412 Ryd converged to within 0.5 mRyd. The number of electrons in the interstitial region in this case was 0.031, the effective dipole charge $+0.181$ a.u. In the case of diamond, the calculation for the lattice parameter value 26.0 a.u. yielded a total energy of -150.044 Ryd converged to within 4 mRyd and 0.017 interstitial electrons. The dipole and interstitial charge values are a consequence of the fact that within the MAPW formalism one cannot dispense with the plane waves altogether. It is encouraging to see how the interstitial contributions decrease. In the case of BN the limit of charge neutrality per atom, if not quite realized, seems to be within reach. For a more precise calculation of atomic energies the correct asymptoticity of the atomic wave functions has to be taken into account. Furthermore in the case of odd electron numbers, as in the B and N atoms, an atomic calculation requires the use of a spin-polarized density functional as discussed by Moruzzi et al. [29] for the case of atoms constituting as metals. For those reasons the values of the cohesion energy calculated within the MAPW formalism have to be viewed as rough estimates. For diamond, the cohesion energy is overestimated by 40%, for BN by 20%. The only consistency observable is the increase of the cohesion energy for the more ionic compound BN, although its actual value of 1.54 eV is again heavily overestimated by the theoretical prediction of 5.25 eV.

In fact, in the case of diamond, the atomic calculations with the appropriate density functional [6] yielded a value of -149.9122 Ryd for two carbon atoms and therefore a cohesion energy of 21.75 eV, which is in fact worse than the value obtained from the MAPW formalism. For B and N, respectively, the spin-polarized atomic calculations [3] provide the values -48.72230 and -108.28804 Ryd, respectively, resulting in a cohesion energy of 20.19 eV, much worse than the MAPW results. However, the difference between the cohesion energies is now improved, having the value 1.56 eV. According to Yin and Cohen [10] an overestimation of the cohesion energy is a common failure of the LDA. This appears to be confirmed by the results of our calculation and the atomic calculations by Gunnarson as cited by Zunger and Freeman [3, 6].

Acknowledgements

Enlightening discussion with Dr. G. M. Fehrenbach and Dr. H. Stöhr are gratefully acknowledged. Further thanks are due to Dr. Stöhr for making available the software packages for the solution of the generalized eigenvalue system with Lagrangean constraints, and to Dr. Fehrenbach for critically reading the manuscript. We owe Prof. Dr. G. Will from the Mineralogical Institute of the University of Bonn considerable thanks for making available to us newer experimental results on the charge distribution of BN.

Appendix

The generalization of the MAPW method, discussed in detail in [15] and [30], to a crystal of arbitrary structure is shortly sketched. Consider a crystal with N nuclei of charge Z_ν at positions $\boldsymbol{R}^\nu$ in the first unit cell and reciprocal lattice vectors $\boldsymbol{K}$. The MAPW wave function reads

$$\psi_{nk}(\boldsymbol{r}) = \sum_{\boldsymbol{K}} v_{\boldsymbol{K}}\, \mathrm{e}^{i(\boldsymbol{k}+\boldsymbol{K})\cdot\boldsymbol{r}} + \sum_{\nu=1}^{N} \sum_{L=(0,1)}^{l_{\max}(\nu)} \vartheta(r_0^\nu - r^\nu)\,(2l+1) \times i^l \eta_l\, \mathrm{e}^{i\boldsymbol{k}\cdot\boldsymbol{R}^\nu}\, \mathscr{P}_L^\nu(r^\nu)\, \mathscr{Y}_L(\boldsymbol{r}^\nu)\,, \tag{A.1}$$

where a finite number of plane waves are employed and $\mathscr{P}_L^\nu$ describes the augmentation within the nonoverlapping APW spheres of radius r_0^ν centered on the nuclear sites: For $l \in \{0, \ldots, l_{\max}(\nu)\}$, the spherical Bessel functions j_l originating from the plane wave expansion within the APW spheres are replaced by suitably chosen solutions R_{sl}^ν, $s \in \{1, \ldots, n_{\max}(l, \nu)\}$ of the radial equation corresponding to the Schrödinger equation within the APW spheres, but including only the spherical component of the potential with respect to $\boldsymbol{R}^\nu$. Thus, the augmented function $\mathscr{P}_L^\nu$ reads

$$\mathscr{P}_L^\nu(r) = \sum_{s=1}^{n_{\max}(l,\nu)} A_{sL\nu} R_{sl}^\nu(r) - \sum_{\boldsymbol{K}} v_{\boldsymbol{K}}\, \mathrm{e}^{i\boldsymbol{K}\cdot\boldsymbol{R}^\nu}\, \mathrm{j}_l(|\boldsymbol{k}+\boldsymbol{K}|\, r)\, \mathscr{Y}_L(\boldsymbol{k}+\boldsymbol{K})\,. \tag{A.2}$$

In equations (A.1) and (A.2) $\mathscr{Y}_L$, where $L = (l, m)$, $l \geqq 0$, $m = 1, \ldots, 2l+1$, stand for the real-valued spherical harmonics. The expansion coefficients $v_{\boldsymbol{K}}$, $A_{sL\nu}$, whose $n, \boldsymbol{k}$-dependence is not explicitly indicated, are obtained by inserting the ansatz (A.2) into the variational principle for Schrödinger's equation, yielding a generalized linear Hermitean eigenvalue problem of finite rank for the Galerkin approximation of the crystal Bloch functions belonging to the propagation vector $\boldsymbol{k}$ in the first BZ. The continuity of the wave function and its first derivative throughout the crystal are ensured by imposing the additional conditions

$$\frac{\mathrm{d}^j}{\mathrm{d}r^j}\, \mathscr{P}_L^\nu(r_0^\nu) = 0 \qquad (j \in \{0, 1\})\,, \tag{A.3}$$

thereby effectively reducing the dimension of the ansatz space. From the eigenvalues and the expansion coefficients, the $\boldsymbol{k}$-gradient of the band energies can then be calculated by application of the Hellmann-Feynman theorem [31, 32]. The latter are needed for the calculation of the total energy and the density of states.

The electron density is obtained from the space group symmetrized one-band densities $\varrho_{nk}^{\mathrm{sym}}$ by discretization of the $\boldsymbol{k}$-integral over the first Brillouin zone using a sufficiently large special point set [20 to 22]. In the case of insulators, this method yields *exact* results when a finite crystal with periodic boundary conditions is considered.

From the electron density and the nuclear point charges at the lattice sites, the one-electron effective potential finally is the sum of two contributions [15, 33]: The first is the Coulomb potential of the charge distribution, obtained by integrating the Poisson equation; the second is the exchange and correlation potential describing many-particle effects in the ground state inhomogeneous electron gas and given by $V_{\mathrm{xc}}(\boldsymbol{r}) = (\delta E_{\mathrm{xc}}/\delta\varrho)\,(\varrho_{\mathrm{el}}(\boldsymbol{r}))$. E_{xc} is a local functional of the electron density; the correlation contribution is parametrized as

described by Gunnarson and Lundqvist [34]. For the applications discussed here we shall generally restrict ourselves to the warped muffin tin (WMT) approximation for the potential, i.e. spherical symmetry of the potential within each APW sphere with respect to its center and arbitrary shape of the potential in the interstitial region. The MAPW formalism then requires the real space representation of the potential only within the APW spheres and a finite number of Fourier coefficients of the potential. The Coulomb contributions to the latter are presented in [33]; the exchange and correlation potential is evaluated by numerical integration.

The self-consistent field is obtained iteratively starting from a crystal potential calculated from superimposed atomic densities. The convergence limit for self-consistency was chosen such that total energy contributions were stable to within about 0.01 mRyd, equivalent to a numerical precision of 8 to 9 digits of the first Fourier coefficients of the potential.

The total energy per unit cell is calculated from the expression given in equation (2.9) of [30]; the generalization to arbitrary crystal structure only requires summation over all atoms in the third term of that equation, replacing Z_c by Z^v and r by $|r - R^v|$. For the materials discussed here we regard E_{tot} as a function of the volume V_c of the unit cell only, limiting ourselves to application of hydrostatic pressure. Such investigations allow to show to what extent the LDA properly describes ground state properties. It is observed that even within the WMT approximation most ground state properties can be evaluated with reasonably good accuracy in the case of zincblende or diamond structures.

References

[1] F. Herman, Phys. Rev. **93**, 1214 (1954).
[2] L. Kleinman and J. C. Phillips, Phys. Rev. **117**, 460 (1960).
[3] A. Zunger and A. J. Freeman, Phys. Rev. B **17**, 2030 (1978).
[4] R. M. Wentzcovich, K. J. Chang, and M. L. Cohen, Phys. Rev. B **34**, 1071 (1986).
[5] Yong-Nian Xu and W. Y. Ching, Phys. Rev. B **44**, 7787 (1991).
[6] A. Zunger and A. J. Freeman, Phys. Rev. B **15**, 5049 (1977).
[7] J. R. Chelikowsky and S. G. Louie, Phys. Rev. B **29**, 3470 (1984).
[8] P. E. Van Camp, V. E. Van Doren, and J. T. Devreese, Phys. Rev. B **34**, 1314 (1986).
[9] M. P. Surh, S. G. Louie, and M. L. Cohen, Phys. Rev. B **43**, 9126 (1991).
[10] M. T. Yin and M. L. Cohen, Phys. Rev. B **24**, 6121 (1981).
[11] Z. W. Lu and A. Zunger, Phys. Rev. B **47**, 15 (1993).
[12] H. Bross, Phys. kondens. Materie **3**, 119 (1964).
[13] H. Bross, Helv. phys. Acta **41**, 717 (1968).
[14] H. Bross, G. Bohn, G. Meister, W. Schubö, and H. Stöhr, Phys. Rev. B **2**, 3098 (1970).
[15] H. Bross and R. Eder, phys. stat. sol. (b) **144**, 175 (1987).
[16] P. J. Dean, E. C. Lightowlers, and D. R. Wright, Phys. Rev. A **140**, 352 (1965).
[17] H. Bross, R. Bader, and G. M. Fehrenbach, SAPW Calculations with Arbitrarily Shaped Potential on Solid Silicon; unpublished.
[18] F. J. Himpsel, J. F. van der Veen, and D. E. Eastman, Phys. Rev. B **22**, 1967 (1980).
[19] F. Nava, C. Canali, C. Jacoboni, and L. Reggiani, Solid State Commun. **33**, 475 (1980).
[20] H. Bross, phys. stat. sol. (b) **179**, 429 (1993).
[21] D. J. Chadi and M. L. Cohen, Phys. Rev. B **8**, 5747 (1973).
[22] D. J. Chadi, Phys. Rev. B **16**, 1746 (1977).
[23] R. J. Weiss, Phil. Mag. **29**, 1029 (1974).
[24] G. Will, A. Kirfel, and B. Josten, unpublished report (1984).
[25] F. D. Murnaghan, Proc. Nat. Acad. Sci. USA **30**, 244 (1944).
[26] E. Knittle, R. M. Wentzcovich, R. Jeanloz, and M. L. Cohen, Nature (London) **337**, 349 (1989).

[27] E. GRÜNEISEN, Ann. Phys. (Leipzig) **16**, 530 (1933).
[28] W. JONES and N. H. MARCH, Theoretical Solid State Physics, Vol. 1, J. Wiley & Sons, Ltd., London 1973.
[29] V. L. MORUZZI, J. F. JANAK, and A. R. WILLIAMS, Calculated Electronic Properties of Metals, Pergamon Press, Inc., London/Oxford 1978.
[30] H. BROSS and R. STRYCZEK, phys. stat. sol. (b) **144**, 675 (1987).
[31] H. HELLMANN, Einführung in die Quantenchemie, Franz Deutike, Leipzig/Wien 1937.
[32] R. P. FEYNMAN, Phys. Rev. **56**, 340 (1939).
[33] G. M. FEHRENBACH and H. BROSS, Phys. Rev. B **48**, 17703 (1993); especially Section II.C.
[34] O. GUNNARSON and B. I. LUNDQVIST, Phys. Rev. B **13**, 4274 (1976).
[35] V. A. FORMICHEV and M. A. RUMSH, J. Phys. Chem. Solids **29**, 1015 (1968).
[36] R. M. CHRENKO, Solid State Commun. **14**, 511 (1974).
[37] H. R. PHILIPP and E. A. TAFT, Phys. Rev. **127**, 159 (1962).
[38] T. TAKAMA, K. TSUCHIYA, K. KOBAYASHI, and S. SATO, Acta cryst. **A46**, 514 (1990).
[39] S. GÖTTLICHER and E. WÖLFEL, Z. Elektrochem **63**, 891 (1959).
[40] H. J. MCSKIMIN and P. ANDREATCH, JR., J. appl. Phys. **43**, 985, 2944 (1972).